

See discussions, stats, and author profiles for this publication at: <https://www.researchgate.net/publication/228439678>

Novel Trisubstituted Harmine Derivatives with Original in Vitro Anticancer Activity

ARTICLE in JOURNAL OF MEDICINAL CHEMISTRY · JULY 2012

Impact Factor: 5.45 · DOI: 10.1021/jm300542e · Source: PubMed

CITATIONS

19

READS

28

10 AUTHORS, INCLUDING:



Céline Bruyère

leucémie espoir recherche

32 PUBLICATIONS 414 CITATIONS

SEE PROFILE



Anders Backlund

Uppsala University

48 PUBLICATIONS 2,031 CITATIONS

SEE PROFILE



Bernard Masereel

University of Namur

194 PUBLICATIONS 3,568 CITATIONS

SEE PROFILE



Robert Kiss

Fonds de la Recherche Scientifique (FNRS)

521 PUBLICATIONS 12,427 CITATIONS

SEE PROFILE

Novel Trisubstituted Harmine Derivatives with Original in Vitro Anticancer Activity

Raphaël Frédérick,^{*,†,||} Céline Bruyère,^{‡,||} Christelle Vancraeynest,[†] Jérémy Reniers,[†] Céline Meinguet,[†] Lionel Pochet,[†] Anders Backlund,[§] Bernard Masereel,[†] Robert Kiss,^{*,‡} and Johan Wouters^{*,†}

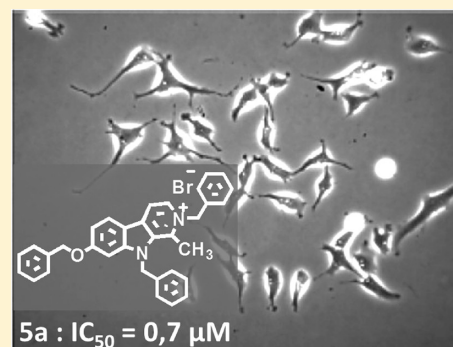
[†]Namur Medicine and Drug Innovation Center (NAMEDIC-NARILIS), University of Namur (FUNDP), 61, Rue de Bruxelles, 5000 Namur, Belgium

[‡]Laboratoire de Toxicologie, Faculté de Pharmacie, Université Libre de Bruxelles (ULB), Boulevard du Triomphe, 1050 Brussels, Belgium

[§]Department of Medicinal Chemistry, Biomedical Centre, Division of Pharmacognosy, Uppsala University, 751 23 Uppsala, Sweden

Supporting Information

ABSTRACT: To overcome the intrinsic resistance of cancer cells to apoptotic stimuli, we designed and synthesized approximately 50 novel β -carbolines structurally related to harmine. Harmine is known for its anticancer properties and is a DYRK1A inhibitor. Of the synthesized compounds, the most active in terms of growth inhibition of five cancer cell lines are cytostatic and approximately 100 times more potent than harmine but demonstrated no DYRK1A inhibitory activity. These novel β -carbolines display similar growth inhibitory activity in cancer cells that are sensitive and resistant to apoptotic stimuli. Using ChemGPS-NP, we found that the more active β -carbolines are all more lipophilic and larger than the less active compounds. Lastly, on the basis of the NCI human tumor cell line anticancer drug screen and the NCI COMPARE algorithm, it appears that some of these compounds, including **5a** and **5k**, seem to act as protein synthesis inhibitors.



■ INTRODUCTION

Cancer is becoming an increasingly important cause of death, and more than 80% of all anticancer drugs target the apoptosis pathways of tumor cells.^{1a–c} However, as emphasized by Wong,^{1c} cancer is a disease in which too little apoptosis occurs, resulting in malignant cells that will not die. In addition, the mechanisms underlying apoptosis are complex and involve multiple pathways in which many defects can occur in cancer cells (e.g., p53 mutations that occur in approximately 50% of cancers²), leading to resistance to anticancer drugs.^{1c} However, drug resistance is also seen in cancers expressing wild-type p53.^{1c} In fact, in addition to defects in the normal regulation of apoptotic pathways, cancer cells also develop resistance to cytotoxic molecules via the activation of membrane transporters that actively pump drugs out of the cells (the so-called “multidrug resistance” (MDR) phenotype), changes in the glutathione system and altered metabolism.^{3a,b} Finally, several cancer types are also able to develop resistance to receptor tyrosine kinase inhibitors (RTKIs), to RTK-targeting antibodies, and to antibodies that inactivate ligands for RTKs.^{3a} Brain cancers (e.g., glioblastoma),^{4a} esophageal cancers,^{4b,c} melanomas,^{4d} pancreatic cancers,^{4e} and non-small-cell lung cancers (NSCLCs)^{4f} are among the cancers associated with the worst prognoses because of their ability to resist most if not all of the current chemotherapies. It should therefore be emphasized that we have made use of glioblastoma and esophageal cancer

models to characterize the in vitro anticancer effects of the compounds developed in this study.

We designed a novel strategy to try to overcome, at least partly, the intrinsic resistance of cancer cells to apoptotic stimuli. We synthesized novel molecules that are structurally related to harmine, which is a naturally occurring β -carboline that was previously isolated from plants, including the Middle Eastern grass harmal or Syrian rue (*Peganum harmala*) and the South American vine ayahuasca (*Banisteriopsis caapi*).^{5a,b} We chose harmine as a scaffold to generate novel derivatives because (i) harmine is associated with anticancer activity,⁶ (ii) harmine has been repeatedly shown to inhibit the protein kinase DYRK1A (dual specificity tyrosine-phosphorylated and regulated kinase 1a),^{7a–c} (iii) overexpression of DYRK1A has been implicated in multiple diseases, tumorigenesis, and uncontrolled cell proliferation,⁸ (iv) harmine-mediated inhibition of DYRK1A induces the activation of caspase-9, which leads to massive apoptosis in different human cell types,^{7c} and (v) melanomas that are intrinsically resistant to apoptotic stimuli overexpress DYRK1A.⁹ In addition, it has been recently shown that harmine can reverse resistance to anticancer drugs by inhibiting the breast cancer resistance protein BCRP.¹⁰

Received: April 17, 2012

Published: July 9, 2012



Table 1. Determination of the in Vitro IC₅₀ Growth Inhibitory Activity Associated with Each Compound That Has Been Cultured for 3 Days in the Presence (or the Absence, Control) of the Various Cancer Cell Lines^a

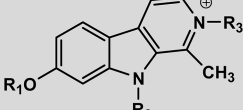
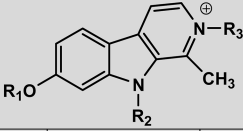
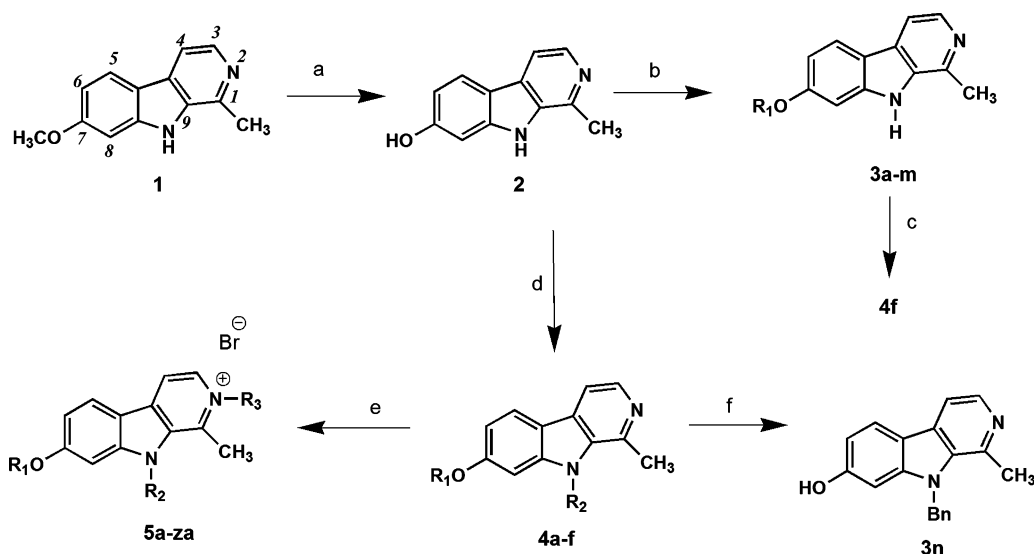
Cmpd	Chemical structure			IC ₅₀ (μM)					
				Glioma cell lines			Oesophageal cancer cell lines		Mean ± SEM
	R1	R2	R3	U373	T98G	Hs683	OE21	OE33	
Harmine 1	CH ₃	H	-	32±2	24±2	37±1	32±2	18±1	28±3
3a	CH ₂ -CH=CH ₂	H	-	32±2	32.0±0.7	28±1	27±2	30±1	30±1
3b	CH ₂ CH(CH ₃) ₂	H	-	24±1	22±3	23±1	12±3	25±1	22±3
3c	(CH ₂) ₂ -OCH ₃	H	-	64±4	61±7	53±6	53±4	66±3	60±3
3d	(CH ₂) ₂ -OH	H	-	42±2	53±3	41±3	30±4	63±4	46±6
3e	(CH ₂) ₃ -CF ₃	H	-	>100	86±11	>100	>100	>100	>80
3f	CH ₂ -cyclohexyl	H	-	7.5±0.1	7.2±0.2	22±2	8.3±0.2	8.1±0.2	11±3
3g	CH ₂ -C ₆ H ₅	H	-	9.3±0.2	17±3	17±2	21±1	4.1±0.6	14±3
3h	(CH ₂) ₂ -C ₆ H ₅	H	-	9.1±0.6	21±1	21±3	14±1	7.9±0.3	15±3
3i	CO-C ₆ H ₅	H	-	27±2	42±3	53±3	30±4	31±4	37±5
3j	CH ₂ -2'-pyridyl	H	-	21±1	20±2	20±1	16±3	23±3	20±1
3k	CH ₂ -3'-pyridyl	H	-	24±1	29±2	30±3	28±2	31±2	29±1
3l	CH ₂ -4'-pyridyl	H	-	2.5±0.2	3.6±0.2	8.1±0.2	5.0±0.4	6.3±0.1	5±1
3m	CH ₂ -naphthyl	H	-	7.4±0.4	12±2	19±2	33±8	8.2±0.4	16±5
3n	H	CH ₂ -C ₆ H ₅	-	80±2	81±11	79±4	35±2	35±2	62±11
4a	CH ₂ -C ₆ H ₅	CH ₂ -C ₆ H ₅	-	18±2	36±2	33±1	28±3	40±4	31±4
4b	3'-fluorobenzyl	3'-fluorobenzyl	-	0.4±0.1	27±1	18±1	7.9±0.2	16±2	14±5
4c	4'-fluorobenzyl	4'-fluorobenzyl	-	30±1	14±2	17±2	15±2	25±2	20±3
4d	CH ₂ -cyclohexyl	CH ₂ -cyclohexyl	-	31±1	32±1	30±2	17±2	15±3	25±4
4e	(CH ₂) ₂ -CH(CH ₃) ₂	(CH ₂) ₂ -CH(CH ₃) ₂	-	33±1	35±1	30±1	30±1	-	32±1
4f	CH ₂ -C ₆ H ₅	(CH ₂) ₂ CH ₃	-	26±1	34±1	13±1	23±1	9±1	21±1
4g	CH ₂ -C ₆ H ₅	H	CH ₂ -C ₆ H ₅	3.9±0.2	5.6±0.2	3.6±0.1	6.0±0.6	5.5±0.3	5±1
5a	CH ₂ -C ₆ H ₅	CH ₂ -C ₆ H ₅	CH ₂ -C ₆ H ₅	0.44±0.0 1	0.48±0.0 2	0.5±0.1	1.3±0.2	0.7±0.1	0.7±0.2
5b	CH ₂ -C ₆ H ₅	CH ₂ -C ₆ H ₅	2'-fluorobenzyl	0.5±0.2	0.37±0.0 1	0.44±0.0 4	0.38±0.0 2	0.70±0.0 8	0.48±0.0 6
5c	CH ₂ -C ₆ H ₅	CH ₂ -C ₆ H ₅	4'-fluorobenzyl	0.6±0.1	0.6±0.1	1.6±0.3	0.61±0.0 4	2.4±0.3	1.2±0.4
5d	CH ₂ -C ₆ H ₅	CH ₂ -C ₆ H ₅	(CH ₂) ₂ -C ₆ H ₅	2.0±0.3	2.4±0.4	2.3±0.1	2.4±0.3	-	2.3±0.1
5e	CH ₂ -C ₆ H ₅	CH ₂ -C ₆ H ₅	(CH ₂) ₂ CH ₃	2.5±0.3	11±1	0.6±0.1	3.4±0.8	-	5±2
5f	CH ₂ -C ₆ H ₅	CH ₂ -C ₆ H ₅	(CH ₂) ₃ CH ₃	0.7±0.1	3.1±0.5	0.6±0.1	1.9±0.3	-	1.5±0.6
5g	CH ₂ -C ₆ H ₅	CH ₂ -C ₆ H ₅	(CH ₂) ₂ -CH(CH ₃) ₂	0.39±0.0 1	1.2±0.2	0.37±0.0 3	0.50±0.0 9	-	0.6±0.2
5h	CH ₂ -C ₆ H ₅	CH ₂ -C ₆ H ₅	(CH ₂) ₂ OH	9±2	61±6	31±3	25±4	-	32±11
5i	3'-fluorobenzyl	3'-fluorobenzyl	CH ₂ -C ₆ H ₅	0.8±0.1	0.97±0.0 2	2.8±0.4	0.4±0.1	2.9±0.1	1.6±0.5
5j	3'-fluorobenzyl	3'-fluorobenzyl	2'-fluorobenzyl	0.6±0.2	0.7±0.2	2.2±0.2	1.4±0.3	3.0±0.2	1.6±0.4
5k	3'-fluorobenzyl	3'-fluorobenzyl	4'-fluorobenzyl	0.9±0.1	1.9±0.3	4.5±0.4	2.9±0.1	3.4±0.1	2.7±0.6

Table 1. continued

Cmpd	Chemical structure			IC ₅₀ (μM)					
				Glioma cell lines			Oesophageal cancer cell lines		Mean ± SEM
	R1	R2	R3	U373	T98G	Hs683	OE21	OE33	
5l	4'-fluorobenzyl	4'-fluorobenzyl	CH ₂ -C ₆ H ₅	0.43±0.0 7	0.40±0.0 4	0.9±0.1	0.5±0.1	1.4±0.1	0.8±0.2
5m	4'-fluorobenzyl	4'-fluorobenzyl	2'-fluorobenzyl	0.5±0.1	0.43±0.0 2	1.2±0.4	1.6±0.3	1.6±0.2	1.1±0.3
5n	4'-fluorobenzyl	4'-fluorobenzyl	4'-fluorobenzyl	2.9±0.1	14±2	13±1	3.7±0.2	3.1±0.3	4.8±0.3
5o	CH ₂ -cyclohexyl	CH ₂ -cyclohexyl	CH ₂ -C ₆ H ₅	0.37± 0.02	0.16±0.0 3	0.38±0.0 1	0.42±0.0 1	0.37±0.0 1	0.34±0.0 5
5p	CH ₂ -cyclohexyl	CH ₂ -cyclohexyl	2'-fluorobenzyl	1.4±0.1	0.07±0.0 1	0.25±0.0 2	0.35±0.0 1	0.35±0.0 2	0.5±0.2
5q	CH ₂ -cyclohexyl	CH ₂ -cyclohexyl	4'-fluorobenzyl	0.04± 0.01	2.0±0.6	3.1±0.3	1.4±0.2	1.0±0.1	1.6±0.4
5r	(CH ₂) ₂ - CH(CH ₃) ₂	(CH ₂) ₂ - CH(CH ₃) ₂	(CH ₂) ₂ OH	2.5±0.3	2.9±0.4	4.0±0.3	7.6±0.3	-	4.0±1
5s	(CH ₂) ₂ - CH(CH ₃) ₂	(CH ₂) ₂ - CH(CH ₃) ₂	(CH ₂) ₂ - CH(CH ₃) ₂	0.22±0.0 3	0.41±0.0 1	0.26± 0.01	0.48±0.0 4	-	0.34±0.0 6
5t	(CH ₂) ₂ - CH(CH ₃) ₂	(CH ₂) ₂ - CH(CH ₃) ₂	CH ₂ -C ₆ H ₅	3.4±0.1	3.5±0.1	3.1±0.1	3.7±0.1	-	3.4±0.1
5u	CH ₂ -C ₆ H ₅	(CH ₂) ₂ CH ₃	CH ₂ -C ₆ H ₅	0.41±0.0 3	1.7±0.5	2.6±0.2	0.57±0.0 8	0.3±0.02	1.1±0.4
5v	CH ₂ -C ₆ H ₅	(CH ₂) ₂ CH ₃	2'-fluorobenzyl	0.39±0.0 1	1.8±0.3	0.45±0.0 2	0.42±0.0 2	0.25±0.0 5	0.7±0.3
5w	CH ₂ -C ₆ H ₅	(CH ₂) ₂ CH ₃	4'-fluorobenzyl	0.88±0.0 6	5.7±0.2	3.1±0.6	1.9±0.3	1.0±0.1	1.5±0.4
5x	(CH ₂) ₂ - CH(CH ₃) ₂	(CH ₂) ₂ - CH(CH ₃) ₂	CH ₂ -C ₆ H ₅	0.38±0.0 5	0.6±0.2	0.47±0.0 5	-	-	0.49±0.0 7
5y	CH ₂ -cyclohexyl	CH ₂ -cyclohexyl	(CH ₂) ₂ OH	1.7±0.5	2.6±0.5	3.8±0.2	-	-	2.7±0.6
5z	CH ₂ -cyclohexyl	CH ₂ -cyclohexyl	(CH ₂) ₂ - CH(CH ₃) ₂	0.4±0.1	0.43±0.0 2	0.42±0.0 6	-	-	0.42±0.0 1
5za	CH ₂ -cyclohexyl	CH ₂ -cyclohexyl	(CH ₂) ₂ -C ₆ H ₅	0.20±0.0 5	0.26±0.0 5	0.31±0.0 3	-	-	0.26±0.0 3

^aThe dash indicates not determined.Scheme 1. Synthesis of β-Carbolines 3a–n, 4a–g, and 5a–za^a

^a(a) HBr, HAc, reflux, overnight; (b) Cs₂CO₃, R₁X, DMF, rt or Δ; (c) 3g, NaH, iodopropane, DMF, 24 h; (d) KOH (5 equiv), DMF, rt, 30 min, then R₁(=R₂)-Br, rt, 24 h (procedure A); (e) R₃-Br (10 equiv), THF, Δ, 48 h (procedure B), or microwave, 155 °C, 4 h (procedure C); (f) 4a, Pd/C (10%), MeOH, rt, 48 h.

Recently, our group reported the inhibitory activity of a series of 7-substituted harmine derivatives against monoamine

oxidase A (MAO-A).¹¹ In the present work, we examined a larger series of compounds and investigated the in vitro growth

Table 2. Pharmacological Analyses of Compounds 1, 3c, 3k, 4a, 4d, 5a, 5k, and 5o

compd	DYRK1A inhibition, IC ₅₀ (μM)	mean in vitro growth inhibition concns determined by MTT colorimetric assay in five human cancer cell line (see Table 1), IC ₅₀ (μM)	global growth ratio (GGR index) (μM) determined by quantitative videomicroscopy in the U373 glioma cell line at the MTT colorimetric assay related IC ₅₀ concn	global profile of the compound in terms of growth inhibition	solubility in PBS, pH 7.4, at rt (μM)
1 (harmine)	0.08 ^a	28 ± 3	0.30 at 32	cytostatic	ND
3c	16	60 ± 3	0.23 at 64	cytostatic	ND
3k	10	29 ± 1	0.29 at 24	cytostatic	ND
4a	16	31 ± 4	0.30 at 18	cytostatic	<3
4d	>10	25 ± 4	0.17 at 31	cytostatic	ND
5a	21	0.7 ± 0.2	0.40 at 0.4	cytostatic	461
5k	<i>b</i>	2.7 ± 0.6	0.53 at 0.9	cytostatic	53
5o	43	0.34 ± 0.05	0.25 at 0.4	cytostatic	123

^aTaken from ref 7a. The DYRK1A IC₅₀ concentration relating to each compound was determined by using 10 concentrations ranging from 10⁻⁴ to 3 × 10⁻⁸ M, in triplicate. Compound 4d was tested in the range 5 × 10⁻⁵ M to 1.5 × 10⁻⁹ M, in triplicate. A radiometric protein kinase assay (³³PanQinaseR activity assay) was used for measuring the kinase activity of DYRK1A protein kinase as detailed in the Experimental Section. ^bNot determined

inhibitory effects of these compounds using both the colorimetric MTT assay^{12a-d} and computer-assisted phase-contrast microscopy (i.e., quantitative videomicroscopy).^{13a-d} Three glioma and two esophageal cancer lines were used for the MTT assays, including the U373 glioma^{12c,14} and the OE21 esophageal^{4c} cancer cell lines that display significant levels of resistance to apoptotic stimuli. Harmine was used as a reference compound. The U373 glioma cell line was used for the quantitative videomicroscopy analyses. Several compounds were also biochemically assayed for their anti-DYRK1A activity. Several of the most potent compounds in terms of in vitro growth inhibitory activity were then evaluated in a 60-cancer-cell-line panel at the NCI (Developmental Therapeutic Program, Division of Cancer Treatment and Diagnosis) in order to compare their mechanism(s) of action to those of the over 763 000 compounds already available in the NCI database.¹⁵ Finally, we used a “ChemGPS-NP” approach,^{16a-c} which is a global physicochemical space model, in order to investigate the region of chemical space where the examined series of compounds are localized.

RESULTS

Chemistry. The monosubstituted derivatives 3a–m (Table 1) were synthesized following a two-step procedure involving the demethylation of harmine (1) to the corresponding harmol (2), followed by realkylation to generate the corresponding 7-substituted β-carboline derivative 3a–m (Scheme 1). The key intermediate 2 was generated via cleavage of the methyl ether present in harmine 1 with hydrobromic acid. The 7-substituted β-carbolines 3a–m were obtained via O-alkylation of 2 in the presence of cesium carbonate with the corresponding alkyl halide. The 7,9-disubstituted compounds 4a–f were obtained via simultaneous O₇- and N₉-alkylation of 2 using 2 equiv of alkyl halide and 5 equiv of potassium hydroxide in DMF. Compound 4a was obtained via reduction using Pd/C. The 2,7,9-trisubstituted β-carboline-2-ium bromides 5a–za were obtained from the corresponding 7,9-disubstituted compound 4 following N₂-alkylation in THF using 10 equiv of the corresponding alkyl bromide. The structure and the purity of each final compound were characterized via ¹H NMR, ¹³C NMR, mass spectrometry (MS), elemental analyses, and HPLC.

Pharmacological Evaluation. Determination of the in Vitro Growth Inhibitory Activity. The growth inhibitory

potency of the approximately 50 synthesized compounds was evaluated in three glioma cell lines (U373, T98G and Hs683¹⁷) and two esophageal cancer cell lines (OE21 and OE33^{4c}) using the MTT assay. The cells were cultured for 3 days in the absence (control) or presence of the synthesized compounds.^{12a-d} Most of the 2,7,9-trisubstituted compounds 5a–za (except 5e, 5h, 5r, and 5t; Table 1) exhibited mean IC₅₀ values at least 10 times lower than that of harmine (1) (Table 1).

Among the 7-monosubstituted β-carbolines 3a–m, the replacement of the 7-CH₃O of harmine with various alkoxy groups 3a–e generated molecules with a mean IC₅₀ ranging from 22 to >100 μM; the IC₅₀ of harmine was 28 μM (Table 1). By contrast, the replacement of the methyl group of harmine (1) by a cyclohexylmethyl 3f, a benzyl 3g, a phenethyl 3h, a 2'- and 4'-pyridyl-CH₂ 3j,l, or a naphthyl-CH₂ slightly augmented the growth inhibitory potency of these compounds when compared to 1 (the mean IC₅₀ ranged from 5 to 20 μM, Table 1).

The addition of a substituent in position 9 decreased the mean growth inhibitory potency when compared with the corresponding 7-monosubstituted β-carbolines (the following pairs of compounds should be compared: 3b/4e, 3f/4d, 3g/4a, and 3g/4f; Table 1). By contrast, the introduction of a second substituent on position 2 increased the in vitro growth inhibitory activity, as demonstrated by the 2,7-dibenzyl-β-carboline 4g (IC₅₀ = 5 μM) when compared with the 7,9-dibenzyl derivative 4a (IC₅₀ = 31 μM) or harmine (1, 28 μM).

Finally, we synthesized β-carbolines bearing substituents in the 2, 7, and 9 positions, 5a–za. Interestingly, apart from 5h that was as potent as 1, all of these trisubstituted molecules were more potent in inhibiting cancer cell line growth than the parent compound with a mean IC₅₀ ranging from 0.3 to 5 μM (Table 1). Compounds 5a, 5b, 5g, 5l, 5o, 5p, 5s, and 5v displayed a mean IC₅₀ in the submicromolar range (Table 1).

As shown in Table 1, the synthesized compounds display in vitro growth inhibitory effects that are similar in cancer cell lines and are sensitive to apoptotic stimuli (Hs683^{12c,14} and OE33^{4c}) or resistant to apoptotic stimuli (U373^{12c,14} and OE21^{4c}). While this finding strongly suggests that the growth inhibitory activity of the compounds is not due to the cytotoxic effects of the compounds or to the induction of apoptosis, quantitative videomicroscopy was used to evaluate the cytostatic and/or cytotoxic activity of selected β-carbolines in the human U373 glioma cell line as detailed below.

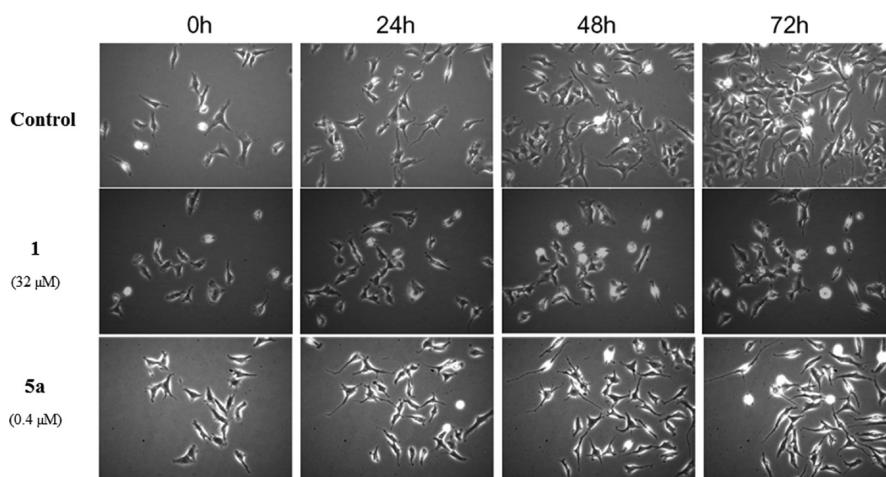


Figure 1. Quantitative videomicroscopy analyses of the in vitro anticancer activity of harmine (**1**) and **5a** in the human U373 glioblastoma cell line. Compounds **1** and **5a** were assayed at their respective in vitro growth inhibitory IC_{50} value, as determined using the MTT assay in U373 glioma cells (see Table 1).

Interestingly, the 2,7,9-trisubstituted β -carboline-2-ium bromides **5** were also characterized by higher aqueous solubility compared to the disubstituted compounds (Table 2, compare **5a**, **5k**, **5o** vs **4a**). This can certainly be attributed to the presence of a permanent positive charge on the trisubstituted compounds.

Evaluation of DYRK1a Kinase Inhibition. As harmine (**1**) has been reported to be a DYRK1A inhibitor, a panel of mono- (**3c,k**), di- (**4a**, **4d**), and tri- (**5a**, **5o**) substituted β -carbolines was selected, and their DYRK1A inhibitory potency was evaluated using a radiometric protein kinase assay (33 PanQinase Activity Assay). These compounds were also analyzed via quantitative videomicroscopy as detailed in the next section. The IC_{50} values for the harmine derivatives were calculated using dose–response curves. These IC_{50} values ranged from 10 to 43 μ M; therefore, these compounds were much less active than harmine (IC_{50} = 0.08 μ M; Table 2). Surprisingly, the two most active compounds (**5a**, **5o**) in terms of growth inhibitory activity in U373 glioma cells (Table 1) were the worst inhibitors of DYRK1A (IC_{50} of 21 and 43 μ M, respectively).

Cytotoxic and Cytostatic Effects of Various Compounds in U373 Glioma Cells. U373 glioma cells were seeded and cultured (T25 cm^2 flasks) for 72 h in the absence (control) or the presence of various β -carbolines at their growth inhibitory IC_{50} (Table 2). The compounds analyzed using quantitative videomicroscopy were those assayed for anti-DYRK1A activity. The quantitative videomicroscopy approach enabled an image of the bottom of the seeded flask to be taken every 4 min over the course of a 72 h observation period.^{13a–d} Thus, 1080 digitized images were available for each experimental condition, which were run in triplicate, and an approximately 40 s movie was generated from these images. These movies clearly demonstrate that the analyzed compounds displayed cytostatic, not cytotoxic, effects in the U373 glioma cells. A morphological illustration of the cytostatic effects induced by **1** and **5a** is provided in Figure 1. For each compound analyzed (Table 2), a global growth ratio (the GGR index) was further calculated, resulting in a value that can be directly compared to the MTT-assay-determined IC_{50} value. First, the global growth (GG) is calculated in each control and in each treated condition by dividing the number of cells on the last image by the number of cells on the first image. The GGR index is obtained for each

compound by dividing the GG values calculated for treated U373 cells by the GG values calculated for the control. As shown in Table 2, the compounds appeared more inhibitory based on their IC_{50} values calculated using the MTT assay when compared with the quantitative videomicroscopy results because the GGR indices were always less than 0.5. This could be because U373 cells grow faster in T25 cm^2 flasks (a final volume of 7 mL) than in 96-well plates (a final volume of 100 μ L). However, even if the IC_{50} values calculated based on the MTT assay resulted in GGR indices less than 0.5, these compounds displayed cytostatic, not cytotoxic, effects (Figure 1, Table 2).

As the most active compounds **5a**, **5k**, **5o** under study in terms of in vitro growth inhibitory activity in U373 glioma cells (Table 1) were the worst inhibitors of DYRK1A (Table 2) while these compounds displayed cytostatic, not cytotoxic, effects (Table 2), we submitted **5k** to a kinase profiling including 358 kinases and 10 lipid kinases (Table 3). At 10 μ M, **5k** decreased by >90% the activity of a dozen of kinases (Table 3) that are implicated in cell proliferation in general and more particularly in tumor cell proliferation, such as CAMK,^{18a,b} MYLK,^{18c} TGF- β receptors,^{18d,e} FER,^{18f} TEC,^{18g} and CSK,^{18h} a feature that can explain at least partly the **5k**-induced cytostatic effects in cancer cells (Table 2). We choose **5k** instead of **5a** or

Table 3. Profiling of **5k** at 10 μ M against 358 Protein Kinases and 10 Lipid Kinases^a

kinase name	kinase family	mean residual activity (%) (duplicate measurements)
STK17A	CAMK	<1
CAMK2A		1
CAMK2D		2
MYLK		2
MYLK2		7
MKNK1		10
TGFB-R1	TKL	6
TGFB-R2		6
FER	TK	7
TEC		8
CSK		10

^aOnly kinases inhibited at >90% are shown.

5o for the kinase profiling because **5k** appeared less toxic in vivo (analyses of the maximal tolerated dose in healthy mice) than **5a** or **5o** (data not shown).

Rationalization of the SAR Analyses. On the basis of these results, we have generated a series of compounds displaying in vitro cytostatic growth inhibitory activity against human cancer cell lines displaying various levels of resistance to apoptotic stimuli at the submicromolar range. Unexpectedly, we also found that these compounds, in fact, did not act as DYRK1A inhibitors. Moreover, structure–activity relationships (SARs) were not easy to infer, as aromatic, substituted or not, and alkyl substituents resulted in molecules with a wide range of activities (mean IC_{50} from 0.34 to 5 μ M). Therefore, to provide a possible explanation for the observed trend in the SAR analyses we reported above, we undertook an analysis using ChemGPS-NP.^{16a–c}

ChemGPS-NP is a global model of chemical property space based on principal component analysis (PCA) that provides a positioning system tuned for the exploration of biologically relevant chemical space (i.e., those areas of chemical space most likely to enclose biologically active compounds). This is achieved by positioning the chemical compound properties using PCA score prediction onto a consistent eight-dimensional (8D) map based on structure-derived physicochemical characteristics for a reference set of compounds.^{16a–c} As with any PCA, the largest variability in data occurs in the first principal component (PC1), with successfully decreasing information content in the following PCs. The first four dimensions of the ChemGPS-NP map, accounting for 77% of data variance, can be interpreted in such a way that PC1 primarily represents size, shape, and polarizability; PC2 corresponds to aromatic- and conjugation-related properties; PC3 describes lipophilicity, polarity, and H-bond capacity; and PC4 expresses flexibility and rigidity.^{16a–c} For a more detailed explanation of ChemGPS-NP chemical property loadings, refer to the work by Rosen et al.^{16c} Any compound, real or virtual, with a known chemical structure can be positioned in ChemGPS-NP property space. From the resulting projections, properties of the compounds, together with trends and clusters of very large data sets, can be compared and easily interpreted. From this analysis (Figure 2), we can see that all of the tested

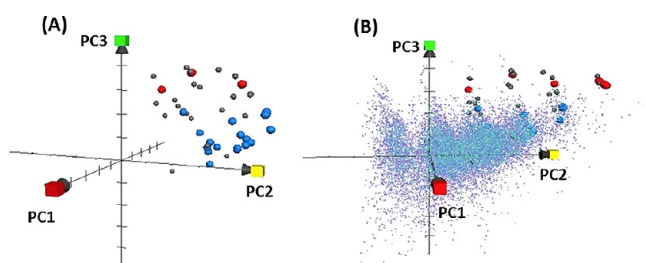


Figure 2. (A) ChemGPS-NP mapping of compounds investigated in the present study. Blue dots indicate the compounds with less in vitro growth inhibitory activity in five human cancer cell lines, and red dots indicate the compounds with more inhibitory activity (see Table 1). (B) ChemGPS-NP mapping of compounds investigated in this study combined with a small reference set of approximately 20 000 compounds from the ZINC-NP database (<http://zinc.docking.org>), which can be considered a simple generalization of “natural products”. The red box indicates PC1 (size, weight, etc.). The yellow box indicates PC2 (aromaticity, rigidity, etc.), and the green box indicates PC3 (lipophilicity, etc.).

β -carbolines are comparably closely positioned in the chemical space; they are not particularly large (PC1 contribution), quite aromatic (PC2 contribution), and lipophilic (PC3 contribution). Interestingly, all the compounds with the greatest in vitro growth inhibitory activity (Tables 1 and 2), represented as red dots in Figure 2, are well separated from the less active compounds, represented as blue dots. The more active compounds are all more lipophilic and larger than the less active compounds, and the degree of aromaticity varies within approximately the same range. If we compare this series of β -carbolines with a set of approximately 20 000 compounds from the ZINC-NP (<http://zinc.docking.org>) database (Figure 2B), which can be seen as a simple generalization of “druglike natural products”, one can see that the derivatives examined in this study are distinct from the majority of the compounds found in the ZINC-NP database. The internal structure visible in the ZINC-NP cloud is mainly due to different degrees of aromaticity.

Analyses of the in Vitro Growth Inhibitory Activity Associated with 5a, 5k, and 5o in the NCI 60-Cancer-Cell-Line Panel. Compounds **5a**, **5k**, and **5o** were first analyzed by the NCI in their 60-cell-line panel at 10 μ M. As shown in Figure 3, revealed with the permission of the NCI, treatment with 10 μ M **5a** resulted in 45% in vitro growth inhibition if the 60 cell lines are taken as a whole (Figure 3A). However, the difference in the magnitude of growth inhibition between the less and more sensitive cancer cell lines at this concentration was over 2 logs (Figure 3A). Quite similar data were obtained for **5k** (data not shown). By contrast, the in vitro growth inhibition profile of 10 μ M **5o** (Figure 3B) differed from the profiles of both **5a** (Figure 3A) and **5k** (data not shown). As shown in Figure 3B, treatment with 10 μ M **5o** resulted in approximately 80% in vitro growth inhibition if the 60 cell lines are taken as whole, and the magnitude of the difference in growth inhibition between the less and the more sensitive cancer cell lines was smaller. These data suggest that **5a** and **5k** could share relatively common mechanism(s) of action, at least in vitro, whereas the mechanism of action of **5o** likely differs from those of **5a** and **5k**, even if the three compounds were clearly identified as cytostatic compounds (Figure 1, Table 2).

We then calculated the “COMPARE correlation coefficients” for **5a**, **5k** and **5o** using the COMPARE software developed by the NCI (Table 4). The highest correlation coefficient for **5a** reached 0.83–0.85 for four compounds whose chemical structures are illustrated in Table 4. The highest coefficient correlation found for **5k** was 0.82 and corresponded to **5a**. The highest correlation coefficient for **5o** reached 0.73–0.78 for four compounds whose chemical structures are also illustrated in Table 4. In the discussion section, we detail the previously described mechanisms underlying the anticancer activity of these compounds, e.g., protein synthesis inhibition. We therefore wanted to validate at the biochemical level the theoretical analyses we performed using the COMPARE approach (Table 4). We thus analyzed by means of Western blotting the effects of **5a** and **5k** (which behave as protein synthesis inhibitors according to the data illustrated in Table 4) and **5o** (which does not behave as a protein synthesis inhibitor according to the data illustrated in Table 4) on the eukaryotic initiation factor 2 (eIF2) in Hs683 oligodendroglioma and U373 glioblastoma cells (Figure 4). The data obtained show that **5a** and **5k** decreased both eIF2 activity (at its phosphorylation levels) and expression in Hs683 and U373 glioma cells after a treatment of 4 h at their respective IC_{50}

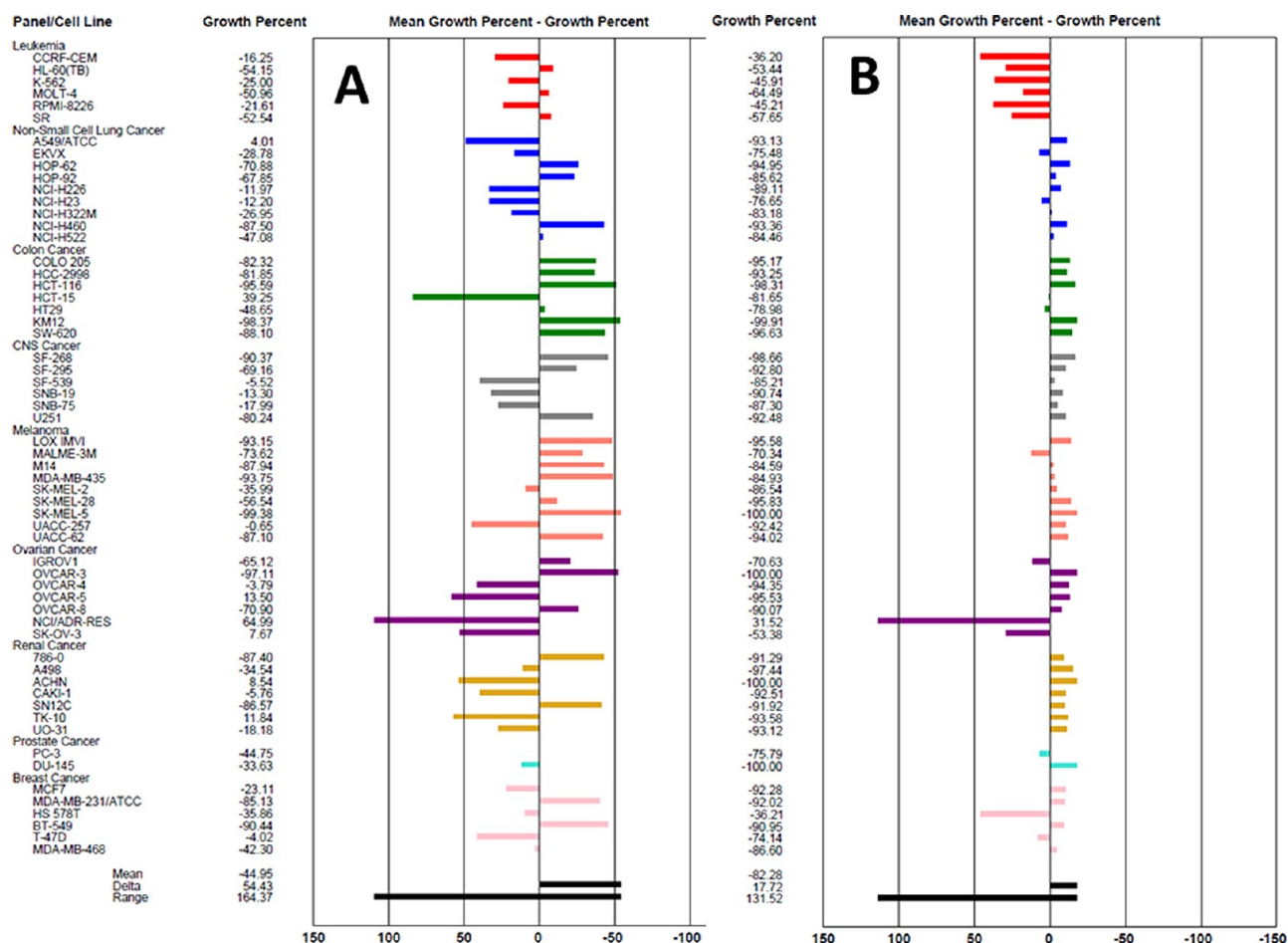


Figure 3. Characterization of the effects induced by 10 μ M **5a** (A) and 10 μ M **5o** (B) in the NCI 60-cell-line panel.

growth inhibitory concentrations (Table 1), while these effects appeared less pronounced, if any, with **5o** using the same experimental conditions (Figure 4).

DISCUSSION AND CONCLUSIONS

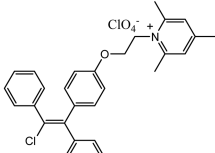
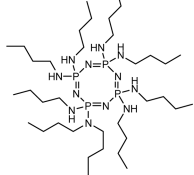
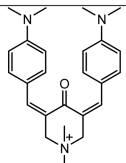
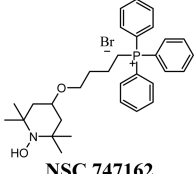
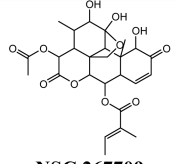
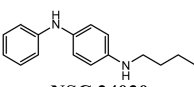
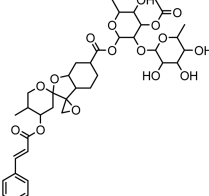
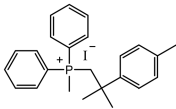
In an attempt to develop compounds to overcome the intrinsic resistance of cancer cells to apoptotic stimuli, we designed and synthesized novel β -carbolines that are structurally related to harmine. Harmine is known for its anticancer properties and is a DYRK1A inhibitor, an enzyme involved in uncontrolled cell proliferation^{7c,8} and cancer cell chemoresistance¹⁰ that is overexpressed in melanomas intrinsically resistant to apoptotic stimuli.⁹

The data we obtained in the current study indicate that we generated cytostatic compounds, with the more potent compounds approximately 2 orders of magnitude more active than harmine in inhibiting cancer cell proliferation. Importantly, these compounds inhibit the growth of apoptosis-resistant cancer cells, with growth inhibitory activity in the submicromolar range, but are weak DYRK1A inhibitors. Profiling the anti-kinase activity of **5k** revealed that **5k**-induced cytostatic effects (Table 2) relate to inhibition of the activity of kinases involved in tumor cell proliferation including a dozen of CAMK, TKL, and TK kinases (Table 3). A 72 h stability study in cell culture medium without serum was performed with **5a** or **5o**, and we recovered greater than 95% of these two compounds (data not shown), suggesting that the cytostatic

effects displayed by **5a** and **5o** are not the result of degradation products.

The β -carbolines we synthesized seem to be located in a distinct chemical space when compared with approximately 20 000 previously analyzed compounds. While the ChemGPS-NP visualization provided initial insights in the physicochemical differences between the more and less active compounds (Figure 2), its full predictive power has not yet been harnessed. This subsequent step would require interpreting the observed physicochemical differences and designing a novel set of harmine derivatives. One interpretational tool that could be used for this purpose is an orthogonal partial least squares discriminant analysis (OPLS-DA), which defines differences in properties between two groups (e.g., more and less active or active and nonactive compounds). The result from an OPLS-DA provides a plot of all 35 descriptors and describes their relative contribution to the differences between the analyzed subsets. With this information, a rational approach to further derivatization can be undertaken. In addition to this analysis, further insights can be gained by continuously predicting derivatives in the ChemGPS-NP chemical property space. This can easily be performed before the actual chemical reactions are performed if an educated guess regarding the structure of the novel product can be made. The SMILES string of the anticipated structure can then be obtained, and the position predicted and evaluated, with regard to the already identified top hits. At present, as shown in Figure 2, all of the most active compounds are significantly more lipophilic (larger values along

Table 4. Correlations of the Differential Cellular Sensitivities in the NCI 60-Cell-Line Screen Using the COMPARE Algorithm^a

Compound 5a		Compound 5o	
Coefficient of correlation	Chemical structure and NSC reference	Coefficient of correlation	Chemical structure and NSC reference
0.85 (n = 48)	 NSC 644614	0.78 (n = 56)	 NSC 58924
0.85 (n = 58)	 NSC 634791	0.73 (n = 58)	 NSC 747162
0.83 (n = 45)	 NSC 267709	0.73 (n = 52)	 NSC 24030
0.83 (n = 45)	 NSC 342443	0.73 (n = 45)	 NSC 176098
0.82 (n = 58)	5k	0.72 (n = 58)	5a

^a“COMPARE correlation coefficients” were generated by a computerized pattern recognition algorithm and serve as an indication of similarities in differential cellular sensitivities of characteristic fingerprints for each compound. The COMPARE coefficient of correlation reported in this table relies on the comparison of the growth inhibitory concentration by 50% (GI₅₀) between “xx” cell lines (indicated in parentheses in Table 4) for either compound **5a** or **5o** versus the >763000 compounds already available in this data base. The four highest correlations found for either **5a** or **5o** among the ≥763000 analyzed compounds are reported in this table. Additional information about the DTP human tumor cell line screen is available at <http://dtp.nci.nih.gov/branches/btb/ivclsp.html>.

PC3) than the less active compounds. Other properties also associated with PC3 apart from lipophilicity are polarity, H-bond capacity, mean electronegativity, and topological polar surface area with regard to N, O, S, and P, with all the latter negatively correlated in a significant way. An initial step to further explore and maybe optimize the harmine derivatives would be to probe if an even larger value along PC3 would result in compounds with even more activity and designing new derivatives with the above aspects. When compared with the small ZINC-NP reference set in Figure 2B, the tested harmine derivatives already display properties that place them on the border of the reference compound cloud. With a larger and more comprehensive set of natural products this is, however, no longer the case, and property-wise, we therefore still move in charted territories.

We requested the help of the Developmental Therapeutic Program (Division of Cancer Treatment and Diagnosis, National Cancer Institute, Rockville, MD, U.S.)¹⁵ to investigate whether the in vitro growth inhibitory activities of β -carbolines **5a**, **5k**, and **5o** match or do not match those of the more than 763 000 compounds already available in the NCI database. Indeed, the NCI has evaluated the in vitro growth inhibitory

profiles of a large number of synthetic compounds, natural products, and plant extracts on 60 different cell lines.¹⁵ The growth inhibitory profile of novel compounds (such as the harmine derivatives examined in the current study) on each of the 60 cell lines is stored in a database that can be analyzed by the COMPARE algorithm, as this program ranks all entries for similarity of growth inhibitory profiles between investigational and reference compounds.¹⁹ The degree of similarity between the growth inhibitory profiles is expressed numerically as a Pearson correlation coefficient (Table 4).¹⁹ As emphasized by Chan et al.,²⁰ the COMPARE algorithm has already been successfully used to identify novel inhibitors of tubulin polymerization,^{21a} inosine monophosphate dehydrogenase,^{21b} topoisomerase I,^{21c} and cyclin-dependent kinases.^{21d} Chan et al.²⁰ used the same approach to search for novel inhibitors of protein synthesis, and they identified 31 known protein synthesis inhibitors, including phyllantoxide and nagilactone C. Using this approach, we found that the four highest Pearson correlation coefficients found for **5a** and **5k** related to protein synthesis inhibitors, including NSC634791, NSC267709 (undulatone), and NSC342443 (phyllantoxide) (Table 4), which are among the 31 protein synthesis inhibitors identified

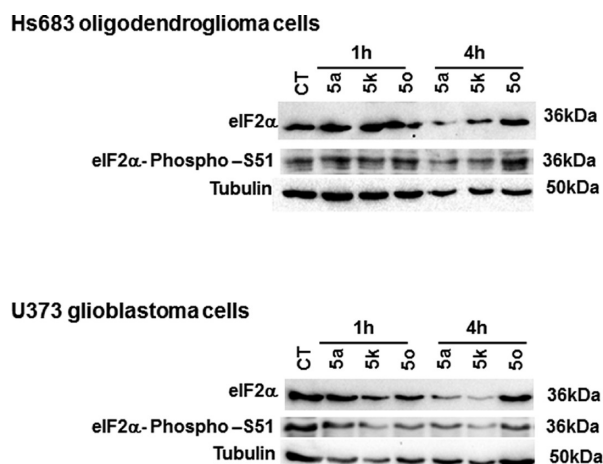


Figure 4. Western blotting analyses of the effects of **5a**, **5k**, and **5o** on the activity (phosphorylation levels) and expression of the eukaryotic initiation factor 2 (eIF2). Each compound was assayed at its IC_{50} growth inhibitory concentration in Hs683 and U373 glioma cells as determined by means of the MTT colorimetric assay (Table 1), i.e., $0.5 \mu M$ **5a**, $5 \mu M$ **5k**, and $0.5 \mu M$ **5o** in Hs683 cancer cells and $0.5 \mu M$ **5a**, $1 \mu M$ **5k**, and $0.5 \mu M$ **5o** in U373 ones.

by Chan et al.²⁰ Phyllantosiide was first isolated from an ethanolic extract prepared from the Central American tree *Phyllanthus acuminatus* based on bioassay-guided cytotoxicity fractionation.²² We did not find any description of the mechanism of action of the fourth compound with a growth inhibitory profile similar to **5a** and **5k**, NSC644614 (Table 4). One of the four compounds with the highest correlation in terms of growth inhibitory profiles when compared with **5o** was NSC747162 (mitotempol), a superoxide dismutase mimetic that interferes with statin activity.²³ Therefore, **5o** does not seem to act as a protein synthesis inhibitor, in contrast to **5a** and **5k**. Western blotting analyses revealed that **5a** and **5k**, but not **5o**, decreased both activity and expression of the eukaryotic initiation factor 2 (eIF2) in Hs683 and U373 glioma cells (Figure 4).

As emphasized by Chan et al.,²⁰ numerous studies have already indicated that deregulation of protein synthesis is a major contributor to cancer initiation and metastatic progression. The overexpression of some initiation factors can lead to malignant transformation, whereas down-regulation of these same factors can suppress the transformed phenotypes. Components of the translation machinery are frequently overexpressed or mutated in cancer cells, and key components of antiapoptotic pathways are also translationally regulated.²⁰ A therapeutic index can be obtained with protein synthesis inhibitors because the transformed cells require higher levels of protein synthesis and because of the translational regulation of some of the proteins involved in cancer progression.²⁰ Again, as emphasized by Chan et al.,²⁰ little effort has been made to systematically search for new inhibitors of eukaryotic protein synthesis, with most of the compounds that are currently used having been identified in chemical screens performed several decades ago.

In conclusion, having generated approximately 50 novel derivatives of harmine, a potent DYRK1A kinase inhibitor, we obtained several compounds that displayed significantly higher growth inhibitory activity than harmine while having lost anti-DYRK1A activity but keeping anti-kinase activity with respect to a dozen of CAMK, TLK, and TK kinases. The most active

compounds from the current study display similar growth inhibitory activity in both cancer cells that are sensitive to apoptotic stimuli and cancer cells that are resistant apoptotic stimuli. Compared with the more than 763 000 compounds already present in the NCI database using the NCI COMPARE analysis, some of these compounds, including **5a** and **5k**, appear to act as protein synthesis inhibitors, a feature that has been biochemically validated with **5a** and **5k** that we showed to inhibit the activity of the eukaryotic initiation factor 2 (eIF2). We are now developing a biochemical assay to determine the mechanism of protein synthesis inhibition associated with each compound we generated in order to derive novel protein synthesis inhibitors with significant therapeutic indices between normal and cancer cells.

EXPERIMENTAL SECTION

Chemistry. Melting points were measured by DSC with a Perkin-Elmer DSC 7.0 Pro apparatus and recorded with Pyris software. NMR spectra were recorded on a Jeol spectrometer (JNM ECX 400). The 1H NMR, ^{13}C NMR, and ^{19}F NMR spectra were recorded at 400, 100, and 376 MHz, respectively. The chemical shifts are reported in parts per million (ppm) relative to the singlet at 7.26 ppm for chloroform in $CDCl_3$, the singlet at 2.50 ppm from dimethyl sulfoxide in $(CD_3)_2SO$, and the singlet at 3.31 ppm for methanol in CD_3OD , and the coupling constants are in Hz. The following abbreviations are used for spin multiplicity: s, singlet; d, doublet; t, triplet; q, quadruplet; qt, quintuplet; m, multiplet; b, broad. Routine thin-layer chromatography (TLC) was performed on silica gel plates (silica gel GF254, VWR). Column chromatography was performed on a Biotage SP1 25+M column (flow of 25 mL/min; spherical particle size 60–200 μm ; MP Biomedicals) equipped with a UV spectrophotometer as a detector (wavelengths of 254 and 320 nm). Solvents from Aldrich and VWR were used without further purification. The purity of the compounds was evaluated via either microanalysis or LC–MS. This information is available in the Supporting Information. Analytical LC–MS analyses were performed on an Agilent 1100 series HPLC coupled with an MSD Trap SL system using UV detection at 220 and 254 nm. Mass spectra were recorded using electron spray ionization (ESI) operating in positive mode. The following methods were used: method A, injection of 10 μL of a 20 $\mu g \cdot mL^{-1}$ solution onto a Agilent Zorbax Eclipse XDB C8 4.6 mm \times 150 mm, 5 μm separation column using a 70:30 solution of 0.01 M butane sulfonate in water/0.01 M butane sulfonate in methanol as the eluent; method B, injection of 5 μL of a 50 μM CH_3CN solution onto a Kinetex Hilic 100 mm \times 2.1 mm, 2.6 μm separation column using a gradient of 100% B to 60% B within 8 min, then reversing to 100% B in 5 min (solution A, 25 mL of a 4% HAc/0.4% trifluoroacetic acid solution diluted in 500 mL water; solution B, 25 mL of a 4% HAc/0.4% trifluoroacetic acid diluted in 500 mL of acetonitrile). All new compounds were determined to be >95% pure by microanalysis or LC–MS.

General Synthetic Procedure A for Simultaneous O_7 - and N_9 -Alkylation of 1-Methyl-7-hydroxy- β -carboline. The 1-methyl-7-hydroxy- β -carboline **2** (500 mg, 1.587 mmol) was dissolved in N,N -dimethylformamide (20 mL), and an amount of 5 equiv of potassium hydroxide was added. The mixture was stirred for 30 min under argon. Then an amount of 2 equiv of the alkyl bromide was added, and the mixture was stirred at room temperature for 24 h under argon. The reaction was followed by TLC (85:15 CH_2Cl_2 /ethanol). At the end of the reaction, the reaction mixture was extracted using dichloromethane (30 mL). The organic layer was washed twice with brine (2×30 mL) and dried with $MgSO_4$, which was collected by filtration. The organic layer was finally evaporated under vacuum to produce the crude product, which was purified via column chromatography as described in the general section with a mobile phase of cyclohexane/ethyl acetate (from 80:20 to 50:50) used as the eluent.

General Synthetic Procedure B for N_9 -Alkylation of 1-Methyl- O_7 -substituted- N_9 -substituted-7-hydroxy- β -carboline. The 1-methyl- O_7 -substituted- N_9 -substituted-7-hydroxy- β -carboline

(100 mg) was dissolved in THF (15 mL). An amount of 10 equiv of alkyl bromide was added, and the mixture was refluxed for 48 h under argon. The reaction was followed by TLC (85:15 CH₂Cl₂/ethanol). At the end of the reaction, the solvents were evaporated under vacuum to produce the crude product, which was further purified via column chromatography as described in the general section with a mobile phase of 95:5 dichloromethane/ethanol used as the eluent.

General Microwave-Assisted Synthetic Procedure C for the N₂-Alkylation of 1-Methyl-O₇-substituted-N₉-substituted-7-hydroxy- β -carboline. The 1-methyl-O₇-substituted-N₉-substituted-7-hydroxy- β -carboline (200 mg) was dissolved in THF (10 mL). An amount of 10 equiv of alkyl halide was added, and the mixture was placed in a microwave reactor at 155 °C for 4 h. At the end of the process, TLC (85:15 CH₂Cl₂/ethanol) was performed. The solvents were then evaporated under vacuum to produce the crude product, which was purified via column chromatography as described in the general section with a mobile phase of dichloromethane/ethanol (from 100:0 to 85:15) used as the eluent.

Syntheses. The synthesis of compounds **2** and **3a–m** has been previously reported.¹¹ A full description of the synthesis of compounds **3n** and **5a–za** can be found in the Supporting Information.

1-Methyl-7-benzoyloxy-9-benzyl- β -carboline (4a). The title compound was synthesized according to the general synthetic procedure A from 1-methyl-7-hydroxy- β -carboline **2** (1.0 g, 3.173 mmol) in the presence of 1-bromomethylbenzene (1.085 g, 6.346 mmol). White powder, yield 66%; *R*_f = 0.88 (CH₂Cl₂/ethanol 85/15); mp 156 °C; *m/z* [MH⁺] 379.2. ¹H NMR (400 MHz, DMSO-*d*₆) δ (ppm): 2.70 (s, 3H, CH₃), 5.14 (s, 2H, O-CH₂), 5.84 (s, 2H, N-CH₂), 6.88 (d, 2H, 2ArH), 6.94 (dd, *J*_{6–5} = 8.7 Hz, *J*_{6–8} = 2.1 Hz, 1H, H-6), 7.17–7.43 (m, 9H, H-8 + 8ArH), 7.89 (d, *J*_{4–3} = 5.0 Hz, 1H, H-4), 8.11 (d, *J*_{5–6} = 8.7 Hz, 1H, H-5), 8.14 (d, *J*_{3–4} = 5.0 Hz, 1H, H-3). ¹³C NMR (100 MHz, DMSO-*d*₆) δ (ppm): 23.2 (CH₃), 47.7 (N-CH₂), 70.2 (O-CH₂), 95.4 (C-8), 110.4 (C-6), 112.9 (C-4), 114.9 (Cq), 123.1 (C-5), 125.8 (2C-ArH), 127.6 (C-ArH), 128.4 (C-ArH), 128.4 (C-ArH), 128.9 (C-ArH), 129.8 (Cq), 129.3 (C-ArH), 135.5 (Cq), 137.3 (Cq), 138.6 (C-3), 139.5 (Cq), 141.3 (Cq), 143.7 (Cq), 160.2 (Cq).

1-Methyl-2-benzyl-7-benzoyloxy-9-benzyl- β -carbolin-2-ium Bromide (5a). The title compound was synthesized according to the general synthetic procedure B from **4a** (0.07 g, 0.185 mmol) in the presence of 1-bromomethylbenzene (0.316 g, 1.850 mmol). Yellow powder; yield 36%; *R*_f = 0.30 (CH₂Cl₂/ethanol 85/15); mp 262 °C; *m/z* [MH⁺] = 469.3. ¹H NMR (400 MHz, DMSO-*d*₆) δ (ppm): 2.81 (s, 3H, CH₃), 5.23 (s, 2H, O-CH₂), 5.96 (s, 2H, N-CH₂), 5.98 (s, 2H, N-CH₂), 6.94 (d, 2H, *J* = 7.1 Hz, ArH), 7.07 (d, 2H, *J* = 7.1 Hz, ArH), 7.18–7.45 (m, 12H, 11 ArH + H-6), 7.53 (s, 1H, H-8), 8.45 (d, 1H, *J*_{5–6} = 8.7 Hz, H-5), 8.69 (d, 1H, *J*_{4–3} = 6.4 Hz, H-4), 8.82 (d, 1H, *J*_{3–4} = 6.2 Hz, H-3). ¹³C NMR (100 MHz, DMSO-*d*₆) δ (ppm): 16.5 (CH₃), 48.8 (N-CH₂), 60.3 (N-CH₂), 70.6 (O-CH₂), 95.5 (C-8), 113.3 (Cq), 114.2 (C-6), 115.2 (C-4), 125.4 (C-5), 125.9 (C-ArH), 127.1 (C-ArH), 128.0 (C-ArH), 128.6 (C-ArH), 128.8 (C-ArH), 129.0 (C-ArH), 129.5 (C-ArH), 129.6 (C-ArH), 133.9 (Cq), 135.2 (Cq), 135.8 (Cq), 136.7 (C-3), 136.7 (Cq), 138.1 (Cq), 140.1 (Cq), 148.5 (Cq), 163.3 (Cq).

1-Methyl-2-(4-fluorobenzyl)-7-(3-fluorobenzyl)oxy-9-(3-fluorobenzyl)- β -carbolin-2-ium Bromide (5k). The title compound was synthesized according to the general synthetic procedure B from **4b** (0.125 g, 0.302 mmol) in the presence of 1-bromomethyl-4-fluorobenzene (0.570 g, 3.020 mmol). Yellow powder; yield 92%; *R*_f = 0.43 (CH₂Cl₂/ethanol 85/15); mp > 200 °C; *m/z* [MH⁺] = 523.1. ¹H NMR (400 MHz, CD₃OD) δ (ppm): 2.90 (s, 3H, CH₃), 5.25 (s, 2H, O-CH₂), 5.92 (s, 2H, N-CH₂), 5.95 (s, 2H, N-CH₂), 6.74 (d, 1H, *J* = 9.6 Hz, ArH), 6.79 (d, 1H, *J* = 7.8 Hz, ArH), 6.97–7.03 (m, 2H, 2ArH), 7.10–7.35 (m, 10H, H-6 + H-8 + 8ArH), 8.37 (d, 1H, *J*_{5–6} = 9.4 Hz, H-5), 8.51 (d, 1H, *J*_{4–3} = 6.4 Hz, H-4), 8.64 (d, 1H, *J*_{3–4} = 6.6 Hz, H-3). ¹³C NMR (100 MHz, CD₃OD) δ (ppm): 15.4 (CH₃), 49.2 (N-CH₂), 59.7 (N-CH₂), 69.4 (O-CH₂), 94.4 (C-8), 112.2 (d, *J* = 23.0 Hz, C-ArH), 113.4 (Cq), 113.8 (d, *J* = 23.0 Hz, C-ArH), 114.4 (C-4 + C-6), 114.5 (d, *J* = 15.3 Hz, 2C-ArH), 115.9 (d, *J* = 22.0 Hz, 2C-ArH), 121.0 (d, *J* = 2.9 Hz, C-ArH), 122.9 (d, *J* = 1.9 Hz, C-ArH), 124.5 (C-

5), 128.8 (d, *J* = 8.6 Hz, 2C-ArH), 130.1 (d, *J* = 7.7 Hz, C-ArH), 130.1 (d, *J* = 2.9 Hz, Cq), 131.0 (d, *J* = 8.6 Hz, C-ArH), 134.6 (Cq), 135.8 (C-3), 136.13 (Cq), 139.2 (d, *J* = 7.7 Hz, Cq), 139.4 (Cq), 139.7 (d, *J* = 6.7 Hz, Cq), 148.5 (Cq), 162.8 (d, *J* = 247.3 Hz, Cq), 163.0 (d, *J* = 245.4 Hz, Cq), 163.4 (d, *J* = 246.3 Hz, Cq), 163.6 (Cq). ¹⁹F NMR (376 MHz, CD₃OD) δ (ppm): −113.5 (s), −114.7 (s), −114.8 (s).

1-Methyl-2-benzyl-7-cyclohexylmethoxy-9-cyclohexyl-methyl- β -carbolin-2-ium Bromide (5o). The title compound was synthesized according to the general synthetic procedure B from **4d** (0.125 g, 0.32 mmol) in the presence of 1-bromomethylbenzene (0.547 g, 3.200 mmol). Yellow powder; yield 74%; *R*_f = 0.33 (CH₂Cl₂/ethanol 85/15); > 200 °C; *m/z* [MH⁺] = 480.3. ¹H NMR (400 MHz, CD₃OD) δ (ppm): 1.07–1.44 (m, 12H, (cyclohexyl)), 1.61–1.95 (m, 10H, (cyclohexyl)), 3.10 (s, 3H, CH₃), 4.00 (d, 2H, *J* = 6.2 Hz, O-CH₂), 4.51 (d, 2H, *J* = 7.3 Hz, N-CH₂), 6.00 (s, 2H, N-CH₂), 7.08 (dd, 1H, *J*_{6–5} = 8.9 Hz, *J*_{6–8} = 2.1 Hz, H-6), 7.15–7.16 (m, 2H, ArH), 7.23 (d, 1H, *J*_{8–6} = 2.1 Hz, H-8), 7.35–7.44 (m, 3H, ArH), 8.25 (d, 1H, *J*_{5–6} = 8.9 Hz, H-5), 8.43 (d, 1H, *J*_{4–3} = 6.6 Hz, H-4), 8.60 (d, 1H, *J*_{3–4} = 6.6 Hz, H-3). ¹³C NMR (100 MHz, CD₃OD) δ (ppm): 15.6 (CH₃), 25.4 (cyclohexyl), 25.6 (cyclohexyl), 25.8 (cyclohexyl), 26.2 (cyclohexyl), 29.5 (cyclohexyl), 30.2 (cyclohexyl), 37.7 (cyclohexyl), 40.2 (cyclohexyl), 51.0 (N-CH₂), 60.4 (N-CH₂), 73.9 (O-CH₂), 94.5 (C-8), 112.7 (Cq), 113.8 (C-4 + C-6), 123.9 (C-5), 126.3 (2C-ArH), 128.5 (C-ArH), 129.2 (2C-ArH), 134.4 (Cq), 134.5 (Cq), 135.4 (C-3), 135.5 (Cq), 139.2 (Cq), 149.1 (Cq), 164.1 (Cq).

Pharmacological Evaluation. Determination of the in Vitro IC₅₀. The colorimetric MTT assay was used, as described previously.^{12a–d} This test measures the number of metabolically active, living cells that are able to transform the yellow product 3-(4,5-dimethylthiazol-2-yl)-2,5-diphenyl tetrazolium bromide (MTT) into the blue formazan dye via mitochondrial reduction. The amount of formazan obtained at the end of the experiment, measured via spectrophotometry, is directly proportional to the number of living cells. Therefore, determination of the optical density enables a quantitative measurement of the effect of the investigated compounds when compared with the control condition (untreated cells) and/or cells treated with other reference compounds.

Five human cancer cell lines (two esophageal cancer and three glioma cell lines) were obtained from either the European Collection of Cell Cultures (ECACC; Salisbury, U.K.) or the American Type Culture Collection (ATCC; Manassas, VA). The two esophageal cancer cell lines were the OE21 squamous (ECACC code 96062201) and the OE33 adenocarcinoma (ECACC code 9607808) cell lines.^{4c} The three glioma cell lines were the Hs683 oligodendroglioma cell line^{12c,14,17,18} (ATCC code HTB-138) and the U373^{12c,14,17,18} (ECACC code 89081403) and T98G^{14,17} (ATCC code CRL-1690) astrogloma cell lines.

To perform the assay, cells (5000–8000 cells/well depending on the cell line examined) were grown in a 96-well, flat-bottomed plate in 100 μ L of medium. Each cell line was seeded in its appropriate culture medium. The detailed experimental procedures are provided elsewhere.^{12a–d} Each experimental condition was run in six replicates.

Computer-Assisted Phase Contrast Microscopy (Quantitative Videomicroscopy). The direct visualization of compound-induced cytotoxic or cytostatic effects was performed as described elsewhere.^{13a–d}

Analyses of DYRK1A Inhibition and Kinase Profiling. The DYRK1A inhibitory activity of the various examined β -carbolines (see Table 2) was performed at ProQinase GmbH (Freiburg, Germany), as detailed previously.^{24a,b} The anti-kinase activity of **5k** was profiled on 358 kinases and 10 lipid kinases also at ProQinase. The materials and methods used by ProQinase to perform the radiometric protein kinase assay (³³PanQinase activity assay) are fully detailed in the Supporting Information of refs 24a and 24b. We originally provided ProQinase with a stock solution of each compound in 100% DMSO, and the aliquots were further diluted with water in 96-well microtiter plates directly before use; 5 μ L of a 2 \times 10⁵ M/10% DMSO solution was transferred to the assay plates. The final volume of the assay was 50 μ L. The concentrations tested for each compound in order to determine the IC₅₀ value are detailed in the legend to Tables 2 and 3.

Western Blott Analyses with the Eukaryotic Initiation Factor 2 (eIF2). We used a modified RIPA buffer to recover the largest part of proteins from Hs683 and U373 glioma cells. This ice cold lysis buffer is composed of 10 mM Tris (pH7.4), 100 mM NaCl, 1 mM EDTA, 1 mM EGTA, 1 mM NaF, 20 mM Na₄P₂O₇, 2 mM Na₃VO₄, 0.1% SDS, 0.5% sodium deoxycholate, 1% Triton-X 100, 10% glycerol, 1 mM AEBSF (Perfabloc, Sigma), 60 µg/mL aprotinin, 10 µg/mL leupeptin, and 1 µg/mL pepstatin.

The control and treated cells were lysed in this buffer and centrifuged for 10 min at 13 000 rpm to eliminate the cellular debris. The concentration of proteins has been determined by the BCA protein assay (ThermoFisher, Erembodegem, Belgium); 35 µg of proteins was loaded onto a denaturing polyacrylamide gel, and after electrophoresis, the proteins were transferred in a PVDF membrane (ThermoFisher). Equal loading and integrity of proteins was verified by means of tubulin immunoblot analysis. The following primary antibodies were used for Western blot analysis: anti-eIF2 α (dilution 1/1000; Abcam; Cambridge, U.K.), anti-eIF2 α S1 (phospho S51) (dilution 1/1000; Abcam), and anti- α tubulin (dilution 1/2000; Abcam). Western blots were developed using the Pierce SuperSignal chemiluminescence system (ThermoFisher) and the Biorad XRS+ system (Biorad, Nazareth, Belgium).

Solubility Measurements. The solubility was evaluated according to a method described previously.²⁵ HPLC measurements were done using method A.

■ ASSOCIATED CONTENT

Supporting Information

Detailed synthesis, characterization, and microanalysis and HPLC purity data of all reported derivatives. This material is available free of charge via the Internet at <http://pubs.acs.org>.

■ AUTHOR INFORMATION

Corresponding Author

*For R.F. (medicinal chemistry): phone, +32 81 72 42 90; e-mail, raphael.frederick@fundp.ac.be. For R.K. (pharmacology): phone, +32 477 62 20 83; e-mail, rkiss@ulb.ac.be. For J.W. (chemistry): phone, +32 81 72 45 50; e-mail, johan.wouters@fundp.ac.be.

Author Contributions

^{||}R.F. and C.B. contributed equally.

Notes

The authors declare no competing financial interest.

■ ACKNOWLEDGMENTS

The authors thank Pierre Legrand and Eduard Dolušić for their assistance. R.F. is a Research Associate of the Fonds de la Recherche Scientifique—FNRS. This project was funded in part by the FNRS Grant FRSM 3.4525.11 and a Télévie Grant 7.4.547.11.F.

■ ABBREVIATIONS USED

ATCC, American Type Culture Collection; DYRK1A, dual-specificity tyrosine-regulated kinase 1A; ECACC, European Collection of Cell Culture; GBM, glioblastoma; MTT, 3-(4,5)-dimethylthiazol-2-yl)-2,5-diphenyltetrazolium bromide; NCI, National Cancer Institute; NSCLC, non-small-cell lung carcinoma; OPLS-DA, orthogonal partial least squares discriminant analysis (sometimes interpreted as orthogonal projection of latent structures); PC1, principal component 1, first dimension in the ChemGPS-NP chemical property space; SAR, structure–activity relationship

■ REFERENCES

- (1) (a) Savage, P.; Stebbing, J.; Bower, M.; Crook, T. Why does cytotoxic chemotherapy cure only some cancers? *Nat. Clin. Pract. Oncol.* **2009**, *6*, 43–52. (b) Wilson, T. R.; Johnston, P. G.; Longley, D. B. Anti-apoptotic mechanisms of drug resistance in cancer. *Curr. Cancer Drug Targets* **2009**, *9*, 307–319. (c) Wong, R. S. Apoptosis in cancer: from pathogenesis to treatment. *J. Exp. Clin. Cancer Res.* **2011**, *30*, 87.
- (2) Martinez-Rivera, M.; Siddik, Z. H. Resistance and gain-of-resistance phenotypes in cancers harboring wild-type p53. *Biochem. Pharmacol.* **2012**, *83* (8), 1049–1062.
- (3) (a) Rosenzweig, S. A. Acquired resistance to drugs targeting receptor tyrosine kinases. *Biochem. Pharmacol.* **2012**, *83* (8), 1041–1048. (b) Rodrigues, A. S.; Dinis, J.; Gromicho, M.; Martins, C.; Laires, A.; Rueff, J. Genomics and cancer drug resistance. *Curr. Pharm. Biotechnol.* **2012**, *13* (5), 651–673.
- (4) (a) Lefranc, F.; Brotchi, J.; Kiss, R. Possible future issues in the treatment of glioblastomas, with a special emphasis on cell migration and the resistance of migrating glioblastoma cells to apoptosis. *J. Clin. Oncol.* **2005**, *23*, 2411–2422. (b) D'Amico, T. A.; Harpole, D. H., Jr. Molecular biology of esophageal cancer. *Chest Surg. Clin. N. Am.* **2000**, *10*, 451–469. (c) Bruyère, C.; Loney, C.; Duray, A.; Cludts, S.; Ruyschaert, J. M.; Saussez, S.; Yeaton, P.; Kiss, R.; Mijatovic, T. Considering temozolomide as a novel potential treatment for esophageal cancer. *Cancer* **2011**, *117*, 2004–2016. (d) Soengas, M. S.; Lowe, S. W. Apoptosis and melanoma chemoresistance. *Oncogene* **2003**, *22*, 3138–3151. (e) Wong, H. H.; Lemoine, N. R. Pancreatic cancer: molecular pathogenesis and new therapeutic targets. *Nat. Rev. Gastroenterol. Hepatol.* **2009**, *6*, 412–422. (f) Han, S.; Roman, J. Targeting apoptotic signaling pathways in human lung cancer. *Curr. Cancer Drug Targets* **2010**, *10*, 566–574.
- (5) (a) Becker, W.; Sippl, W. Activation, regulation, and inhibition of DYRK1A. *FEBS J.* **2011**, *278*, 246–256. (b) Wegiel, J.; Gong, C. X.; Hwang, Y. W. The role of DYRK1A in neurodegenerative diseases. *FEBS J.* **2011**, *278*, 236–245.
- (6) Cao, R.; Chen, H.; Peng, W.; Ma, Y.; Hou, X.; Guan, H.; Liu, X.; Xu, A. Design, synthesis and in vitro and in vivo antitumor activities of novel beta-carboline derivatives. *Eur. J. Med. Chem.* **2005**, *40*, 991–1001.
- (7) (a) Bain, J.; Plater, L.; Elliott, M.; Shapiro, N.; Hastie, C. J.; McLauchlan, H.; Klevernic, I.; Arthur, J. S.; Alessi, D. R.; Cohen, P. The selectivity of protein kinase inhibitors: a further update. *Biochem. J.* **2007**, *408*, 297–315. (b) Gockler, N.; Fofre, G.; Papadopoulos, C.; Soppa, U.; Tejedor, F. J.; Becker, W. Harmine specifically inhibits protein kinase DYRK1A and interferes with neurite formation. *FEBS J.* **2009**, *276*, 6324–6337. (c) Seifert, A.; Allan, L. A.; Clarke, P. R. DYRK1A phosphorylates caspase 9 at an inhibitory site and is potentially inhibited in human cells by harmine. *FEBS J.* **2008**, *275*, 6268–6280.
- (8) Laguna, A.; Aranda, S.; Barallobre, M. J.; Barhoum, R.; Fernandez, E.; Fotaki, V.; Delabar, J. M.; de la Luna, S.; de la Villa, P.; Arbones, M. L. The protein kinase DYRK1A regulates caspase-9-mediated apoptosis during retina development. *Dev. Cell* **2008**, *15*, 841–853.
- (9) De Wit, N. R.; Burtscher, H. J.; Weidle, U. H.; Ruiter, D. J.; van Muijen, G. N. Differentially expressed genes identified in human melanoma cell lines with different metastatic behavior using high density oligonucleotide arrays. *Melanoma Res.* **2002**, *12*, 57–69.
- (10) Ma, Y.; Wink, M. The beta-carboline alkaloid harmine inhibits BCRP and can reverse resistance to the anticancer drugs mitoxantrone and camptothecin in breast cancer cells. *Phytother. Res.* **2010**, *24*, 146–149.
- (11) Reniers, J.; Robert, S.; Frederick, R.; Masereel, B.; Vincent, S.; Wouters, J. Synthesis and evaluation of beta-carboline derivatives as potential monoamine oxidase inhibitors. *Bioorg. Med. Chem.* **2011**, *19*, 134–144.
- (12) (a) Dumont, P.; Ingrassia, L.; Rouzeau, S.; Ribaucour, F.; Thomas, S.; Roland, I.; Darro, F.; Lefranc, F.; Kiss, R. The Amarylidae isocarboxystyryl narciclasine induces apoptosis by activation of the death receptor and/or mitochondrial pathways in

cancer cells but not in normal fibroblasts. *Neoplasia* **2007**, *9*, 766–776. (b) Mathieu, V.; De Nève, N.; Le Mercier, M.; Dewelle, J.; Gaussin, J. F.; Dehoux, M.; Kiss, R.; Lefranc, F. Combining bevacizumab with temozolomide increases the antitumor efficacy of temozolomide in a human glioblastoma orthotopic xenograft model. *Neoplasia* **2008**, *10*, 1383–1392. (c) Ingrassia, L.; Lefranc, F.; Dewelle, J.; Pottier, L.; Mathieu, V.; Spiegl-Kreinecker, S.; Sauvage, S.; El Yazidi, M.; Dehoux, M.; Berger, W.; Van Quaquebeke, E.; Kiss, R. Structure–activity relationship analysis of novel derivatives of narciclasine (an Amaryllidaceae isocarboxystyl derivative) as potential anticancer agents. *J. Med. Chem.* **2009**, *52*, 1100–1114. (d) Lamoral-Theys, D.; Andolfi, A.; Van Goietsenoven, G.; Cimmino, A.; Le Calvé, B.; Wauthoz, N.; Mégalizzi, V.; Gras, T.; Bruyère, C.; Dubois, J.; Mathieu, V.; Kornienko, A.; Kiss, R.; Evidente, A. Lycorine, the main phenanthridine Amaryllidaceae alkaloid, exhibits significant antitumor activity in cancer cells that display resistance to proapoptotic stimuli: an investigation of structure–activity relationship and mechanistic insight. *J. Med. Chem.* **2009**, *52*, 6244–6256.

(13) (a) Delbrouck, C.; Doyen, I.; Belot, N.; Decaestecker, C.; Ghanooni, R.; de Lavarelle, A.; Kaltner, H.; Choufani, G.; Danguy, A.; Vandenhoven, G.; Gabius, H. J.; Hasid, S.; Kiss, R. Galectin-1 is overexpressed in nasal polyps under budesonide and inhibits eosinophil migration. *Lab. Invest.* **2002**, *82*, 147–158. (b) Lefranc, F.; Mijatovic, T.; Mathieu, V.; Rorive, S.; Decaestecker, C.; Debeir, O.; Brothi, J.; Van Ham, P.; Salmon, I.; Kiss, R. Characterization of gastrin-induced proangiogenic effects in vivo in orthotopic U373 experimental human glioblastomas and in vitro in human umbilical vein endothelial cells. *Clin. Cancer Res.* **2004**, *10*, 8250–8265. (c) Mathieu, V.; Pirker, C.; Martin de Lasalle, E.; Vernier, M.; Mijatovic, T.; De Nève, N.; Gaussin, J. F.; Dehoux, M.; Lefranc, F.; Berger, W.; Kiss, R. The sodium pump alpha-1 subunit: a disease progression-related target for metastatic melanoma treatment. *J. Cell. Mol. Med.* **2009**, *13*, 3960–3972. (d) Van Goietsenoven, G.; Hutton, J.; Becker, J. P.; Lallemand, B.; Robert, F.; Lefranc, F.; Pirker, C.; Vandenbussche, G.; Van Antwerpen, P.; Evidente, A.; Berger, W.; Prévost, M.; Pelletier, J.; Kiss, R.; Kinzy, T. G.; Kornienko, A.; Mathieu, V. Targeting of eEF1A with Amaryllidaceae isocarboxystyls as a strategy to combat melanomas. *FASEB J.* **2010**, *24*, 4575–4584.

(14) Branle, F.; Lefranc, F.; Camby, I.; Jeuken, J.; Geurts-Moespot, A.; Sprenger, S.; Sweep, F.; Kiss, R.; Salmon, I. Evaluation of the efficiency of chemotherapy in in vivo orthotopic models of human glioma cells with and without 1p19q deletions and in C6 rat orthotopic allografts serving for the evaluation of surgery combined with chemotherapy. *Cancer* **2002**, *95*, 641–655.

(15) Developmental Therapeutic Program, Division of Cancer Treatment and Diagnosis, National Cancer Institute, Rockville, MD, U.S. <http://dtp.cancer.gov>.

(16) (a) Larsson, J.; Gottfries, J.; Bohlin, L.; Backlund, A. Expanding the ChemGPS chemical space with natural products. *J. Nat. Prod.* **2005**, *68*, 985–991. (b) Larsson, J.; Gottfries, J.; Muresan, S.; Backlund, A. ChemGPS-NP: tuned for navigation in biologically relevant chemical space. *J. Nat. Prod.* **2007**, *70*, 789–794. (c) Rosen, J.; Lövgren, A.; Kogej, T.; Muresan, S.; Gottfries, J.; Backlund, A. ChemGPS-NP_{Web}: chemical space navigation online. *J. Comput.-Aided Mol. Des.* **2009**, *23*, 253–259.

(17) (a) Belot, N.; Rorive, S.; Doyen, I.; Lefranc, F.; Bruyneel, E.; Dedecker, R.; Micik, S.; Brothi, J.; Decaestecker, C.; Salmon, I.; Kiss, R.; Camby, I. Molecular characterization of cell substratum attachments in human glial tumors relates to prognostic features. *Glia* **2001**, *36*, 375–390. (b) Sivasankaran, B.; Degen, M.; Ghaffari, A.; Hegi, M. E.; Hamou, M. F.; Ionescu, M. C.; Zweifel, C.; Tolnay, M.; Wasner, M.; Mergenthaler, S.; Miserez, A. R.; Kiss, R.; Lino, M. M.; Merlo, A.; Chiquet-Ehrismann, R.; Boulay, J. L. Tenascin-C is a novel RBPJ κ -induced target gene for Notch signaling in gliomas. *Cancer Res.* **2009**, *69*, 458–465.

(18) (a) Yang, B. F.; Xiao, C.; Roa, W. H.; Krammer, P. H.; Hao, C. Calcium/calmodulin-dependent protein kinase II regulation of c-FLIP expression and phosphorylation in modulation of Fas-mediated signaling in malignant glioma cells. *J. Biol. Chem.* **2003**, *278*, 7043–

7050. (b) Takai, N.; Ueda, T.; Nasu, K.; Yamashita, S.; Toyofuku, M.; Narahara, H. Targeting calcium/calmodulin-dependence kinase I and II as a potential anti-proliferation remedy for endometrial carcinomas. *Cancer Lett.* **2009**, *277*, 235–243. (c) Han, Y. J.; Ma, S. F.; Yourek, G.; Park, Y. D.; Garcia, J. G. A transcribed pseudogene of MYLK promotes cell proliferation. *FASEB J.* **2011**, *25*, 2305–2312. (d) Horbelt, D.; Denkis, A.; Knaus, P. A portrait of transforming growth factor beta superfamily signaling: background matters. *Int. J. Biochem. Cell Biol.* **2012**, *44*, 469–474. (e) Wang, P.; Yu, J.; Yin, Q.; Li, W.; Ren, X.; Hao, X. Rosiglitazone suppresses glioma cell growth and cell cycle by blocking the transforming growth factor-beta mediated pathway. *Neurochem. Res.* [Online early access]. DOI: 10.1007/s11064-012-0828-8. Published Online: **2012**. (f) Zoubeydi, A.; Rocha, J.; Zouanat, F. Z.; Hamel, L.; Scarlata, E.; Aprikian, A. G.; Chevalier, S. The Fer tyrosine kinase cooperates with interleukin-6 to activate signal transducer and activator of transcription 3 and promote human prostate cancer cell growth. *Mol. Cancer Res.* **2009**, *7*, 142–155. (g) Wang, S. Y.; Li, F. F.; Zheng, H.; Yu, K. K.; Ni, F.; Yang, X. M.; Qu, C. K.; Li, J. Rapid induction and activation of Tec tyrosine kinase in liver regeneration. *J. Gastroenterol. Hepatol.* **2006**, *21*, 668–673. (h) Feng, X.; Lu, X.; Man, X.; Zhou, W.; Jiang, L. Q.; Knyazev, P.; Lei, L.; Huang, Q.; Ullrich, A.; Zhang, Z.; Chen, Z. Overexpression of Csk-binding protein contributes to renal cell carcinogenesis. *Oncogene* **2009**, *28*, 3320–3331.

(19) Paull, K. D.; Shoemaker, R. H.; Hodes, L.; Monks, A.; Scudiero, D. A.; Rubinstein, L.; Plowman, J.; Boyd, M. R. Display and analysis of patterns of differential activity of drugs against human tumor cell lines: development of mean graph and COMPARE algorithm. *J. Natl. Cancer Inst.* **1989**, *81*, 1088–1092.

(20) Chan, J.; Khan, S. N.; Harvey, I.; Merrick, W.; Pelletier, J. Eukaryotic protein synthesis inhibitors identified by comparison of cytotoxicity profiles. *RNA* **2004**, *10*, 528–543.

(21) (a) Gharehbaghi, K.; Paul, K.; Kelley, J. J.; Barchi, J. J., Jr.; Marquez, V. E.; Cooney, D. A.; Monks, A.; Scudiero, D.; Kohn, K.; Jayaram, H. N. Cytotoxicity and characterization of an active metabolite of benzamide riboside: a novel inhibitor of IMP dehydrogenase. *J. Cancer* **1994**, *56*, 892–899. (b) Cleaveland, E. S.; Monks, A.; Vaigro-Wolff, A.; Zaharevitz, D. W.; Paull, K.; Ardalán, K.; Cooney, D. A.; Ford, H., Jr. Site of action of two novel pyrimidine biosynthesis inhibitors accurately predicted by the COMPARE program. *Biochem. Pharmacol.* **1995**, *49*, 947–954. (c) Kohlhaagen, G.; Paull, K.; Cushman, M.; Nagafuji, P.; Pommier, Y. Protein-linked DNA strand breaks induced by NSC314622: a novel non-camptothecin topoisomerase I poison. *Mol. Pharmacol.* **1998**, *54*, 50–58. (d) Zaharevitz, D. W.; Gussio, R.; Loest, M.; Senderowicz, A. M.; Lahusen, T.; Kunick, C.; Meijer, L.; Sausville, E. A. Discovery and initial characterization of the paullones: a novel class of small-molecule inhibitors of cyclin-dependent kinases. *Cancer Res.* **1999**, *59*, 2566–2569.

(22) Kupchan, S. M.; LaVoie, E. J.; Branfman, A. R.; Fei, B. Y.; Bright, W. M.; Bryan, R. F. Phyllantocin, a novel bisabolane aglycone from the antileukemic glycoside, phyllantoside. *J. Am. Chem. Soc.* **1977**, *99*, 3199–3201.

(23) Choi, H. C.; Song, P.; Xie, Z.; Wu, Y.; Xu, J.; Zhang, M.; Dong, Y.; Wang, S.; Lau, K.; Zou, M. H. Reactive nitrogen species is required for the activation of the AMP-activated protein kinase by statin in vivo. *J. Biol. Chem.* **2008**, *283*, 20186–20197.

(24) (a) Lamoral-Theys, D.; Pottier, L.; Kerff, F.; Dufrasne, F.; Proutière, F.; Wauthoz, N.; Neven, P.; Ingrassia, L.; Van Antwerpen, P.; Lefranc, F.; Gelbcke, M.; Pirotte, B.; Kraus, J. L.; Nève, J.; Kornienko, A.; Kiss, R.; Dubois, J. Simple di- and trivanillates exhibit cytostatic properties toward cancer cells resistant to pro-apoptotic stimuli. *Bioorg. Med. Chem.* **2010**, *18*, 3823–3833. (b) Lamoral-Theys, D.; Wauthoz, N.; Heffeter, P.; Mathieu, V.; Jungwirth, U.; Lefranc, F.; Nève, J.; Dubois, J.; Dufrasne, F.; Amighi, K.; Berger, W.; Gailly, P.; Kiss, R. Trivanillic polyphenols with anticancer cytostatic effects through the targeting of multiple kinases and intracellular Ca²⁺ release. *J. Cell. Mol. Med.* **2012**, *16*, 1421–1434.

(25) Dolusic, E.; Larrieu, P.; Moineaux, L.; Stroobant, V.; Pilotte, L.; Colau, D.; Pochet, L.; Van den Eynde, B.; Masereel, B.; Wouters, J.; Frederick, R. Tryptophan 2,3-dioxygenase (TDO) inhibitors. 3-(2-(Pyridyl)ethenyl)indoles as potential anticancer immunomodulators. *J. Med. Chem.* **2011**, *54* (15), 5320–5334.